JVI Journals.ASM.org

Distinct Transformation Tropism Exhibited by Human T Lymphotropic Virus Type 1 (HTLV-1) and HTLV-2 Is the Result of Postinfection T Cell Clonal Expansion

Priya Kannian,[a,b] Han Yin,[a,b] Rami Doueiri,[a,b] Michael D. Lairmore,[a,b,c,d] Soledad Fernandez,[e] and Patrick L. Green[a,b,c,d]

Center for Retrovirus Research, The Ohio State University, Columbus, Ohio, USA[a]; Department of Veterinary Biosciences, The Ohio State University, Columbus, Ohio, USA[b]; Department of Molecular Virology, Immunology, and Medical Genetics, The Ohio State University, Columbus, Ohio, USA[c]; Comprehensive Cancer Center and Solove Research Institute, The Ohio State University, Columbus, Ohio, USA[d]; and Center for Biostatistics, The Arthur James Cancer Hospital and Research Institute, The Ohio State University, Columbus, Ohio, USA[e]

Human T lymphotropic virus type 1 (HTLV-1) and HTLV-2 are related but pathogenically distinct viruses. HTLV-1 mainly causes adult T cell leukemia, while HTLV-2 is not associated with leukemia. *In vitro*, HTLV-1 and HTLV-2 predominantly transform CD4$^+$ and CD8$^+$ T cells, respectively: the genetic determinant maps to the viral envelope. Herein, we investigate whether this transformation tropism occurs during initial infection or subsequently during the cellular transformation process. Since most individuals are chronically infected at the time of detection, we utilized an established rabbit model to longitudinally measure the early HTLV-1 and HTLV-2 infection and replication kinetics in purified CD4$^+$ and CD8$^+$ T cells. HTLV-1 and HTLV-2 were detected in both CD4$^+$ and CD8$^+$ T cells within 1 week postinoculation. In HTLV-1-infected rabbit CD4$^+$ T cells, proviral burden and *tax*/*rex* mRNA expression peaked early, and expression levels were directly proportional to each other. The late expression of the antisense transcript (*Hbz* or *Aph-2*) correlated directly with a late proviral burden peak in HTLV-1- or HTLV-2-infected rabbit CD8$^+$ T cells, respectively. This study provides the first *in vivo* evidence that these viruses do not exhibit cellular preference during initial infection. We further evaluated the transformation tropism of HTLV-1 and HTLV-2 over a 9-week period using *in vitro* cell growth/immortalization assays. At the early weeks, both HTLV-1 and HTLV-2 showed proportionate growth of CD4$^+$ and CD8$^+$ T cells. However, beyond week 5, the predominance of one particular T cell type emerged, supporting the conclusion that transformation tropism is a postinfection event due to selective clonal expansion over time.

Human T lymphotropic viruses (HTLVs) are complex deltaretroviruses (34). To date, HTLV type 1 (HTLV-1) and HTLV-2 are the most extensively characterized. HTLV-1 infects 15 to 25 million people worldwide (35) and mainly causes adult T cell leukemia (ATL) and a neurological disorder, HTLV-1-associated myelopathy/tropical spastic paraparesis (HAM/TSP) (6, 15, 32, 46). HTLV-2 is less prevalent and less pathogenic; infected individuals sporadically develop neurologic disorders and demonstrate marginal lymphocytosis, but so far there has been no evidence of leukemia (1, 3, 31). Both virus strains have been detected in a variety of hematopoietic cells from infected individuals (12, 20, 22, 25, 37). However, HTLV-1 and HTLV-2 preferentially transform T cells in culture; HTLV-1 predominantly transforms CD4$^+$ T cells, while HTLV-2 mainly transforms CD8$^+$ T cells (41, 42, 45). This *in vitro* preference is clinically apparent with HTLV-1, as ATL is a CD4$^+$ T cell malignancy. Even though CD4$^+$ T cells are the primary target cells for HTLV-1 transformation, CD8$^+$ T cells have been shown to carry a higher proviral burden than CD4$^+$ T cells in HAM/TSP patients and asymptomatic carriers (18, 27, 28). HTLV-2 proviral burden also has been shown to be higher in CD8$^+$ T cells in infected individuals (28). HTLV-1 proviral loads have been directly correlated with neurological disease severity (38). These results suggest that CD4$^+$ T cells and CD8$^+$ T cells are key players in pathogenesis. Understanding the ability of HTLV-1 and HTLV-2 to infect and persist in these two T cell populations during the early infection stage will provide insights into their distinct pathogenic differences.

Using a panel of HTLV-1 and HTLV-2 recombinant viruses, we previously showed that the HTLV envelope is the genetic determinant that dictates the differential HTLV-1 and HTLV-2 transformation tropism in cell culture (42). This finding instigated the exploration of differential cellular receptor complexes responsible for the entry and, potentially, postentry events of the virus. A number of studies have shown that the HTLV-1 envelope requires heparan sulfate proteoglycan (HSPG) and neuropilin 1 (NRP-1) for binding to the host cell and glucose transporter 1 (GLUT-1) for entry (7, 8, 17, 26, 33). The HTLV-2 envelope requires GLUT-1 and NRP-1 for both binding and entry; virus binding is not dependent on and is actually inhibited by increased levels of HSPG (7, 17). Jones et al. reported that HSPG expression on CD4$^+$ T cells and GLUT-1 expression on CD8$^+$ T cells are increased especially upon cell activation, although CD4$^+$ and CD8$^+$ T cells express both HSPG and GLUT-1 (17). Taken together, the data have led to the hypothesis that this tropism, dictated by differential receptor interactions, may be a contributing factor to the distinct pathogenesis of HTLV-1 and HTLV-2.

The main function of the viral envelope is to facilitate entry of the virus into new target cells. However, it remains unclear whether the distinct transformation tropism of HTLV-1 and

Received 23 November 2011 **Accepted** 12 January 2012
Published ahead of print 25 January 2012
Address correspondence to Patrick L. Green, green.466@osu.edu.
P. Kannian and H. Yin contributed equally to this article.

doi:10.1128/JVI.06900-11

HTLV-2 conferred by the viral envelope is at the level of entry or occurs later during the infection or cell expansion process. Here, we investigate if the potential preference of a particular T cell type, $CD4^+$ or $CD8^+$ T cells, for HTLV-1- or HTLV-2-mediated transformation, respectively, is dictated at the early infection stage, utilizing the well-established *in vivo* rabbit model (5, 21, 43). Initial infection by HTLV is generally asymptomatic, and typically the asymptomatic carriers are infected for an unknown period of time prior to detection. Therefore, the *in vivo* rabbit model facilitates the evaluation of T cell tropism at the time of initial infection. Our longitudinal 12-week rabbit inoculation study revealed that HTLV-1 or HTLV-2 provirus was detected as early as week 1 in both $CD4^+$ and $CD8^+$ T cells using real-time PCR, indicating there was no tropism difference between the two viruses at the infection stage. The possibility that this preferential tropism occurs during the transformation process was determined using our standard *in vitro* cell growth/immortalization assay (30, 41, 42, 45). The longitudinal 9-week *in vitro* immortalization assay revealed an early proliferation of both $CD4^+$ and $CD8^+$ T cells irrespective of the virus strain and a late selection and outgrowth of the preferred T cell type, indicating that the predominance of a particular T cell type occurs during the clonal expansion process. Taken together, our findings from the *in vivo* rabbit study as well as the *in vitro* immortalization assay indicate that the witnessed preferential transformation tropism is not dictated at the initial infection stage, but is the result of selective clonal expansion over time as part of the transformation process, which likely corresponds to the decades-long clinical latency period in HTLV-1-infected people.

MATERIALS AND METHODS

Cell lines and plasmids. 729Achneo and 729pH6neo are stable HTLV-1 and HTLV-2 producer cell lines that were generated and characterized previously (42). The parental 729 B cell line was used as the negative control. All three cell lines were maintained in Iscove's Dulbecco's minimum essential medium (Cellgro; Mediatech, Manassas, VA). Human peripheral blood mononuclear cells (PBMCs) were isolated using Ficoll-Paque (GE Life Sciences, Piscataway, NY) and cultured with virus producer cell lines in RPMI 1640 (Gibco, Invitrogen, Grand Island, NY) and 10 U/ml recombinant human interleukin-2 (rhIL-2; Roche Applied Biosciences, Indianapolis, IN). All media were supplemented with 10% fetal calf serum (Gemini Bio-Products, Sacramento, CA), 2 mM L-glutamine (Gibco, Invitrogen, Grand Island, NY), 100 U/ml penicillin, and 100 μg/ml streptomycin (Gibco, Invitrogen, Grand Island, NY). The real-time PCR assays utilized proviral or cDNA plasmid clones containing the *gag*/*pol* (ML760 and pH6neo) and *tax*/*rex* (SE356 and IY531) sequences from both HTLV-1 and HTLV-2, respectively, *Hbz* sequence from HTLV-1 (JA662), *Aph-2* sequence from HTLV-2 (HY1018), and rabbit glyceraldehyde-3-phosphate dehydrogenase (GAPDH; ML789) as standards to quantitate copy numbers. The plasmids containing the above sequences (except *Aph-2*) have been described previously (23). HY1018 was generated in a pME-18S vector using the PCR-amplified sequence from the HTLV-2 proviral plasmid pH6neo flanked by EcoRI and NotI restriction sites; the PCR product contained the partial noncoding region of 5′ *Aph-2* (nucleotides [nt] 8562 to 8558), exon 1 (nt 8557 to 8545), and exon 2 (nt 7173 to 6635). The plasmid standards were stored as single-use aliquots at −20°C.

Rabbit inoculation. Three groups of 12-week-old New Zealand White (NZW) male rabbits (four rabbits per group) were inoculated intravenously through the lateral ear vein with approximately 10^7 gamma-irradiated (10,000 rads) 729Achneo cells (HTLV-1 group) or 729pH6neo cells (HTLV-2 group), with the actual cell number equilibrated for p19 Gag production in the viral supernatant (p19 Gag output was approximately 800 pg/ml from one million healthy virus producer cells in 24 h), or 729 cells (control group). Approximately 15 ml of peripheral blood was collected from the central ear artery at week 0 (preinoculation bleed) and at weeks 1, 2, 4, 8, and 12 (postinoculation bleeds). Complete blood counts were determined by autoanalyzer, and $CD4^+$ and $CD8^+$ T cell counts were measured by flow cytometry. Heparinized blood was processed for isolation of plasma, and PBMCs were isolated using a Percoll gradient (1.083 g/ml; Sigma-Aldrich Corp., St. Louis, MO). Plasma was tested for antibody responses against HTLV Gag and Env proteins using the modified line Western blot assay (MP Biomedicals, Solon, OH) as described previously (24).

DNA and RNA extraction from purified $CD4^+$ and $CD8^+$ T cells. At each time point, rabbit PBMCs were stained with purified mouse anti-rabbit CD4 antibody (clone Ken-4; AbD Serotech, MorphoSys UK, Ltd., Kidlington, Oxford, United Kingdom) followed by biotin-conjugated secondary rat anti-mouse IgG2a/2b antibody (clone R2-40; BD Biosciences, San Jose, CA). $CD4^+$ T cells were isolated using streptavidin-labeled FlowComp beads as described by the manufacturer (Dynal, Invitrogen, Grand Island, NY). $CD8^+$ T cells also were purified similarly from the above unbound fraction using primary mouse anti-rabbit CD8 antibody (clone 12.57; AbD Serotech, MorphoSys UK, Ltd., Kidlington, Oxford, United Kingdom) and secondary biotin-conjugated rat anti-mouse IgG1 (clone A85-1; BD Biosciences, San Jose, CA). DNA and RNA were extracted simultaneously from the beads using the Allprep DNA/RNA extraction kit (Qiagen, Valencia, CA) according to the manufacturer's instructions. RNA was subjected to on-column DNase treatment (2.8 U/ml; Qiagen, Valencia, CA), and cDNA was made immediately both with and without reverse transcriptase enzyme using the First Strand cDNA synthesis kit (Invitrogen, Grand Island, NY). DNA was used for detecting the proviral load, and cDNA was used for gene expression analysis by real-time PCR.

TaqMan-based real-time PCR. The primers used for all the sequences except *Aph-2* were described previously (23). The primers and TaqMan probe for detecting the *Aph-2* sequence (nucleotide numbers correspond to pH6neo proviral plasmid) were RTPAPH-2-S (5′-^{8562}AGAGGATGGATC CCCAAG^{8545}^{7173}ACT^{7171}-3′), RTPAPH-2-AS (5′-^{7110}GGAGGCACACC AGATGTCAGA^{7130}-3′), and TMPAPH-2 (5′-6-carboxyfluorescein [FAM]-^{7168}TTTAGGAGATTGCCGTTAGGAGACCAGGG^{7140}-6-carboxytetramethylrhodamine[TAMRA]-3′). For the real-time PCR, all samples were tested in duplicate. The samples and standards were amplified initially with DNA (105 ng) or cDNA in a 25-μl PCR mixture containing 300 nM each primer. The cycling profile for this round of PCR was a single cycle of 94°C for 10 min followed by 20 cycles of 94°C for 30s, 55°C for 30s, and 72°C for 40s and a single-cycle final extension of 72°C for 5 min. This PCR product was amplified in a 15-μl real-time PCR mixture containing 300 nM and 100 nM concentrations of the corresponding primers and TaqMan probes, respectively. The cycling profile for the second round of real-time PCR was a single cycle of 94°C for 3 min followed by 40 cycles of 94°C for 15 s, 55°C for 30 s, and 72°C for 40s. For GAPDH, only the latter 40-cycle real-time PCR was performed. The analytical detection limit of the primers was determined to be one DNA copy with plasmid standards. This sensitivity translated to 1 in 2,000 cells for the detection of both DNA and RNA of *gag*/*pol* from stably transfected cells (729Achneo and 729pH6neo cells). The copy numbers of the proviral loads extrapolated from the corresponding standard curves were expressed as proviral loads per cell based on the experimental calculation that 1 μg of extracted PBMC DNA is approximately equivalent to 134,600 cells. The mRNA copy numbers were normalized to 10^6 copies of cellular GAPDH.

Immortalization assay. Approximately 10^6 729Achneo cells (wild-type HTLV-1 [wtHTLV-1]), 729pH6neo cells (wtHTLV-2), normalized for p19 Gag production in the viral supernatant, or 729 cells (negative control) were gamma-irradiated (10,000 rads) and cocultured with 2×10^6 freshly isolated normal human PBMCs in 24-well plates. For 8 to 10 weeks, the cultures were fed with the same media as described above and monitored by measuring viability using the Trypan blue exclusion test

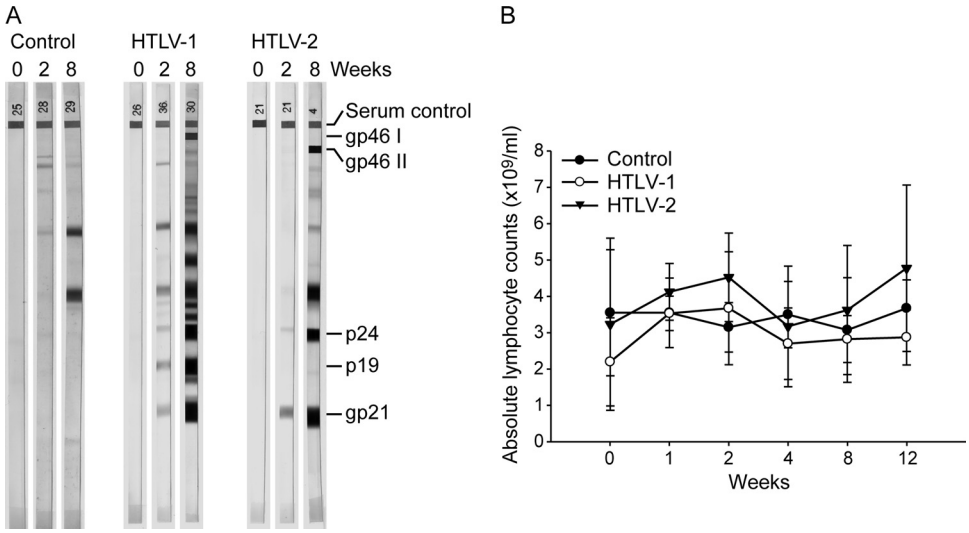

FIG 1 Establishment of persistent infection in rabbits. (A) The line blot assay results from one representative rabbit in each of the three groups are shown at weeks 0, 2, and 8. The topmost band is an IgG serum control band. The HTLV-1/2 Gag proteins are represented by p24 and p19 bands. The HTLV-1 envelope surface protein is represented by the gp46 I band. The HTLV-2 envelope surface protein is represented by the gp46 II band. The gp21 band represents the transmembrane component of the HTLV-1/2 envelope. (B) Shown is the average of the absolute lymphocyte counts with the standard deviations among the four rabbits in each of the three groups at the tested time points. The closed circles are the control rabbits, the open circles are the HTLV-1-infected rabbits, and the inverted triangles are the HTLV-2-infected rabbits.

and p19 Gag production using an enzyme-linked immunosorbent assay (ELISA) (ZeptoMetrix, Buffalo, NY), on a weekly basis. Every week, eight wells per wild type were harvested and stained using fluorescein isothiocyanate (FITC)-conjugated anti-human CD3, phycoerythrin (PE)-conjugated anti-human CD4, and allophycocyanin (APC)-conjugated anti-human CD8 antibodies (BD Biosciences, San Jose, CA) by flow cytometry. At 9 weeks, all remaining wells were phenotyped as described above.

Statistical analyses. The correlations between the proviral loads and gene expression levels in the serial samples were calculated using SigmaPlot linear regression coefficients (*r* values), and the corresponding two-tailed *P* values were calculated using the statistical calculator of VassarStats (Vassar College, Poughkeepsie, NY). The proviral loads between the two HTLV-1- and HTLV-2-infected groups were compared by *t* test using the SigmaPlot statistical calculator. The normalized percentages of the proliferating T cells at each week in the wtHTLV-1- and wtHTLV-2-immortalized cultures were compared using a generalized linear model that included the following factors: virus group (wtHTLV-1 and wtHTLV-2), time, and the interaction of the two main effects. The *P* values of the pairwise comparisons at each week were adjusted by Tukey's method.

RESULTS

HTLV-1 or HTLV-2 infection of rabbits. Twelve-week-old NZW male rabbits were inoculated with irradiated 729 cells, 729Achneo cells, or 729pH6neo cells. Peripheral blood was collected at pre- and postinoculation time points longitudinally. To confirm the establishment of HTLV-1 or HTLV-2 infection in the rabbits, plasma was tested for antibodies against HTLV Gag and Env proteins. Figure 1A shows the humoral responses of one representative rabbit from each of the three groups at 0, 2, and 8 weeks postinoculation. Weak antibody reactions against these proteins were detected as early as week 2 in all HTLV-inoculated rabbits; however, they were strongly positive at all subsequent time points. The four control rabbits did not elicit a detectable humoral response at any of the time points tested. To determine the effect of HTLV-1 or HTLV-2 infection on the various hematologic parameters, we analyzed EDTA-anticoagulated blood from control and HTLV-infected rabbits for complete blood counts and differential white blood cell counts. Both groups of HTLV-1- and HTLV-2-infected rabbits exhibited modest lymphocytosis at weeks 1 and 2 (Fig. 1B). There were no statistically significant differences in any of the hematologic parameters tested at any given time point among the three groups (data not shown). The $CD4^+$ and $CD8^+$ T-cell counts from each rabbit were determined by flow cytometry. There were no significant differences in the numbers of $CD4^+$ and $CD8^+$ T cells between the control and HTLV-infected groups at any given time point (data not shown). Thus, the viral infection, as assessed by the various hematologic parameters, at these early time points mimics the asymptomatic infection in humans (28).

HTLV-1 and HTLV-2 infection in $CD4^+$ T cells. The $CD4^+$ T cell is the primary target T cell in ATL patients and is also the preferred transformation target *in vitro* (13, 37, 42). HTLV-2 has been detected in $CD4^+$ T cells from infected individuals with very high proviral loads (38). However, HTLV-2 predominately transforms $CD8^+$ T cells *in vitro*. *In vivo*, HTLV-2 has not been associated with leukemia. In a quest to understand differential infection and replication abilities of HTLV-1 and HTLV-2 in $CD4^+$ T cells, we determined the proviral loads over a 12-week postinoculation period in purified $CD4^+$ T cells obtained from the four HTLV-1- or HTLV-2-infected rabbits. The purity of the isolated $CD4^+$ T cell population by positive antibody selection was determined to be 90% using flow cytometry (data not shown). We note that this purified $CD4^+$ T cell population may contain a very small percentage of monocytes that are capable of being infected by HTLV-1 or HTLV-2, albeit at much lower efficiency than T lymphocytes (25). Both DNA and RNA were extracted from this purified $CD4^+$ T cell population. Real-time PCR using 105 ng of DNA was performed with the corresponding *gag*/*pol* primers to

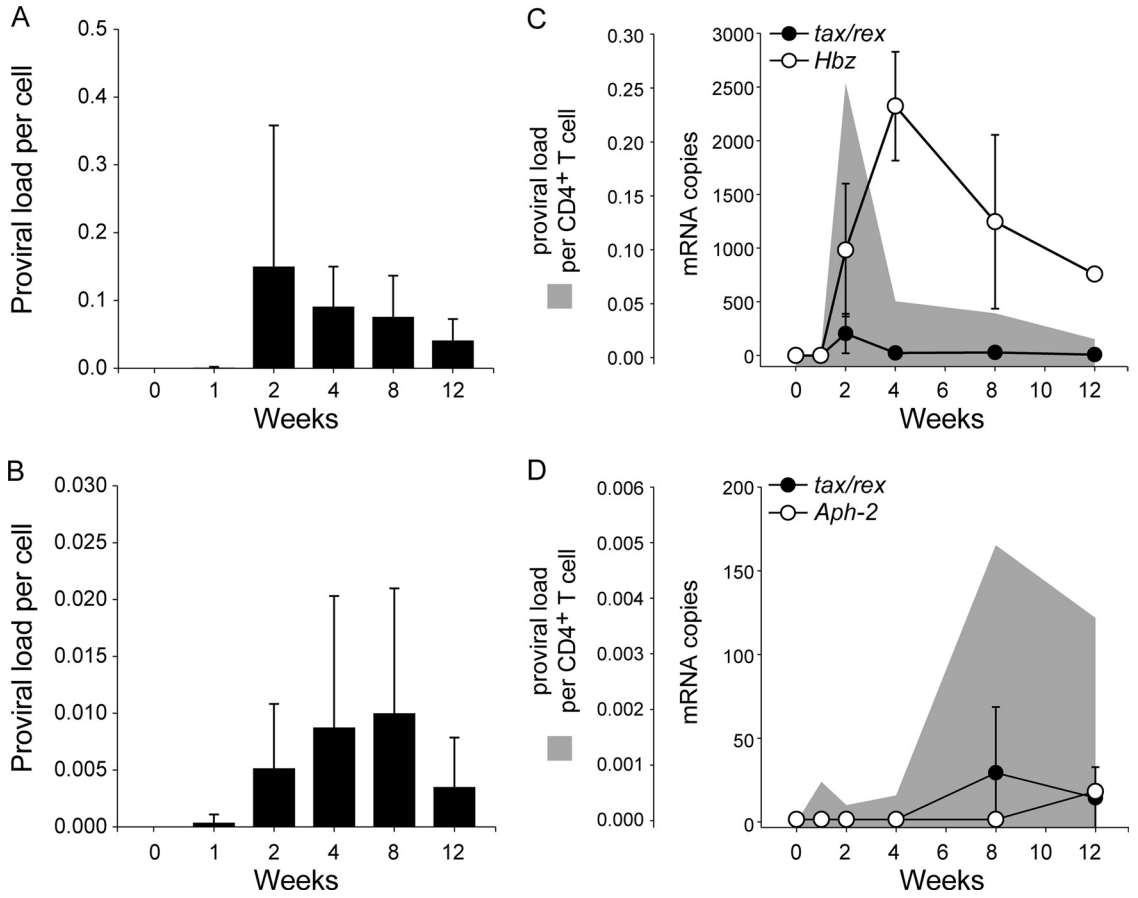

FIG 2 HTLV-1 and HTLV-2 infection in the $CD4^+$ T cells. (A) Average HTLV-1 proviral burden per cell from the four rabbits plotted against the tested time points in weeks. The error bars depict the standard deviations for each bar. (B) Average HTLV-2 proviral burden per cell from the four rabbits plotted against the tested time points in weeks. The error bars depict the standard deviations for each bar. (C) Average expression levels of *tax*/*rex* (closed circles) and *Hbz* (open circles) mRNA in 2/4 HTLV-1-infected rabbits are shown as line plots superimposed over the average proviral loads (gray area plots) from the corresponding rabbits. The error bars depict the standard deviations for each symbol on the line plots. (D) The average expression levels of *tax*/*rex* (closed circles) and *Aph-2* (open circles) mRNA in 2/4 HTLV-2-infected rabbits are shown as line plots superimposed over the average proviral loads (gray area plots) from the corresponding rabbits. The error bars depict the standard deviations for each symbol on the line plots. For better visualization of the trend, the graphs have been plotted at various scales.

quantitate proviral loads. The proviral loads in the control rabbits were below background levels in the $CD4^+$ T cells.

The average HTLV-1 and HTLV-2 proviral loads from the corresponding infected rabbits are shown in Fig. 2A and B, respectively. Provirus was detected as early as week 1 in both HTLV-1 (1 in 1,250 cells)- and HTLV-2 (1 in 2,500 cells)-infected groups. By week 2, the proviral loads peaked in HTLV-1-infected rabbits (1 in 7 cells) and then subsequently began to decline. In contrast, in the HTLV-2-infected rabbits, the proviral load continued to rise until week 8 (1 in 100 cells). The average maximum proviral loads were 14-fold higher in HTLV-1-infected rabbits than in HTLV-2-infected rabbits. By week 12, the proviral loads of HTLV-1 (1 in 25 cells) and HTLV-2 (1 in 200 cells) had declined in the $CD4^+$ T cells.

Due to the evidence supporting a key role for Tax (which mediates viral transcription and is essential for cellular transformation) and the antisense strand-carried gene *Hbz* (which facilitates viral persistence and cellular proliferation) in the HTLV-1 leukemogenic process, we next measured the *tax*/*rex* mRNA and the expression levels of the *Hbz* (HTLV-1) and *Aph-2* (HTLV-2) antisense transcripts in 2/4 inoculated rabbits from each group using real-time reverse transcription-PCR (RT-PCR). The average mRNA expression levels from the HTLV-1- and HTLV-2-infected rabbits are shown as line plots superimposed over the average proviral loads of the corresponding rabbits, shown as gray area plots in Fig. 2C and D, respectively. In the HTLV-1-infected rabbits, *tax*/*rex* mRNA expression peaked very early, by week 2, similar to the proviral loads. Therefore, *tax*/*rex* mRNA expression was directly proportional to the proviral loads ($r = 1.0$, $P < 0.0001$). Since there was a time lag in the *Hbz* mRNA expression levels in these cells, its expression did not correlate with the proviral loads. In the HTLV-2-infected group, the *tax*/*rex* mRNA expression levels also peaked with the proviral loads, but in contrast to the HTLV-1-infected group, this did not occur until 8 weeks postinfection. The virus burden and gene expression levels were quite low, but there was no significant correlation between these parameters in the HTLV-2 group. *Aph-2* expression was detected at low levels only at week 12.

Taken together, these data clearly show that HTLV-1 had a higher infection rate in the $CD4^+$ T cells than HTLV-2. Over time,

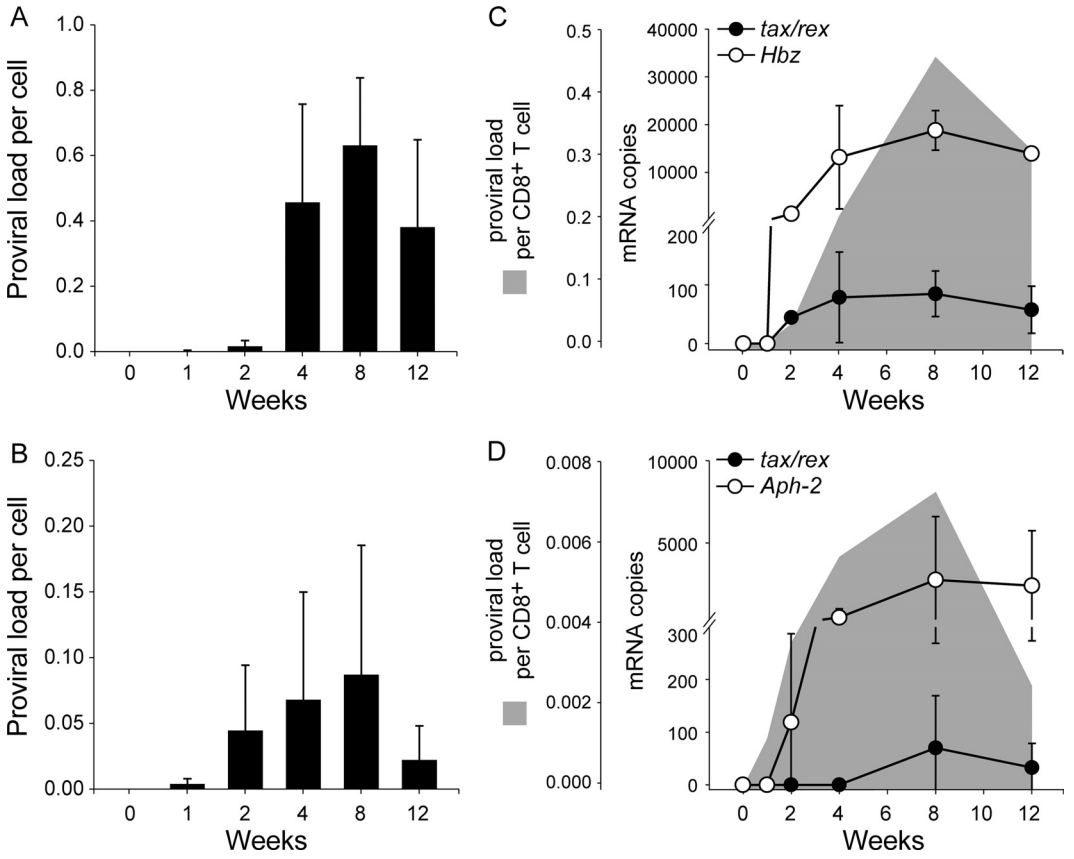

FIG 3 HTLV-1 and HTLV-2 infection in the $CD8^+$ T cells. (A) The average HTLV-1 proviral burden per cell from the four rabbits plotted against the tested time points in weeks. The error bars depict the standard deviations for each bar. (B) The average HTLV-2 proviral burden per cell from the four rabbits plotted against the tested time points in weeks. The error bars depict the standard deviations for each bar. (C) The average expression levels of *tax*/*rex* (closed circles) and *Hbz* (open circles) mRNA in 2/4 HTLV-1-infected rabbits are shown as line plots superimposed over the average proviral loads (gray area plots) from the corresponding rabbits. The error bars depict the standard deviations for each symbol on the line plots. (D) The average expression levels of *tax*/*rex* (closed circles) and *Aph-2* (open circles) mRNA in 2/4 HTLV-2-infected rabbits are shown as line plots superimposed over the average proviral loads (gray area plots) from the corresponding rabbits. The error bars depict the standard deviations for each symbol on the line plots. For better visualization of the trend, the graphs have been plotted at various scales.

the proviral load pattern varied between the two viruses, with the HTLV-1 burden reaching maximum levels 6 weeks earlier than HTLV-2. As expected, in both groups, the *tax*/*rex* mRNA expression pattern matched that of the proviral loads, consistent with the important role of Tax in viral transactivation and replication. In the HTLV-1-infected group, consistent with previous reports, *tax*/*rex* mRNA is downregulated after initial infection, by week 4, followed by upregulation of *Hbz* mRNA, which likely allows escape of the infected cell from immune surveillance, thereby facilitating viral persistence.

HTLV-1 and HTLV-2 infection in $CD8^+$ T cells. In both HTLV-1- and HTLV-2-infected individuals, $CD8^+$ T cells carry a higher proviral burden than $CD4^+$ T cells (18, 27, 28). It is interesting to note that in ATL patients, the $CD4^+$ T cells are transformed in spite of a higher proviral burden in the $CD8^+$ T cells during the long latency period. To understand the infection and replication kinetics of HTLV-1 and HTLV-2 in the $CD8^+$ T cells of a newly infected host, we simultaneously purified $CD8^+$ T cells from the control or HTLV-1- or HTLV-2-infected rabbits. The purity of the isolated population was also 90% (data not shown). Similar to the $CD4^+$ T cells, the isolated $CD8^+$ T cell population was subjected to DNA and RNA extractions, followed by real-time PCR and RT-PCR for the determination of proviral loads and gene expression levels. As expected, the proviral loads and gene expression levels in the control rabbits were below background levels.

The average proviral loads in the $CD8^+$ T cells over the 12-week period are shown in Fig. 3A and B for HTLV-1- and HTLV-2-infected rabbits, respectively. Similar to the $CD4^+$ T cells, the HTLV-1 (1 in 1,000 cells) and HTLV-2 (1 in 200 cells) proviral burdens were detected as early as week 1 postinoculation. In both groups, the pattern of proviral burden was the same over time, where there was a peak by week 8 followed by a decline by week 12. This general pattern was similar to that observed in $CD4^+$ T cells from HTLV-2-infected rabbits. At week 8, the average maximum proviral loads in $CD8^+$ T cells were 7-fold higher in HTLV-1-infected rabbits (1 in 1.7 cells) than in HTLV-2-infected rabbits (1 in 11 cells); this difference was statistically significant ($P = 0.003$).

We then determined the expression profile of *tax*/*rex* mRNA and the *Hbz* (HTLV-1) and *Aph-2* (HTLV-2) antisense transcripts in the $CD8^+$ T cells from 2/4 inoculated rabbits (Fig. 3C and D). In the HTLV-1-infected rabbits, the *tax*/*rex* mRNA expression levels (shown as closed circles) peaked at week 4, followed by a subsequent peak in the proviral loads (shown as gray area plot) at week

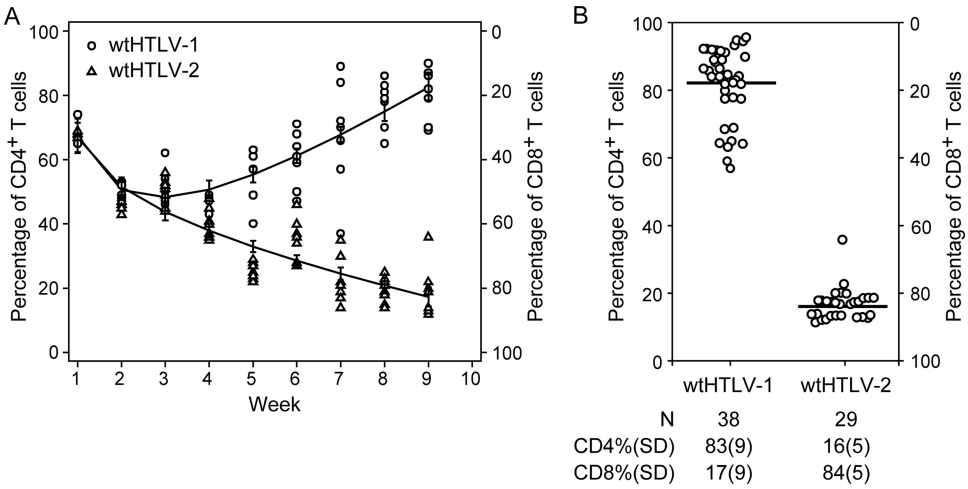

FIG 4 HTLV-1- and HTLV-2-induced immortalization of $CD4^+$ and $CD8^+$ T cells. Gamma-irradiated 729Achneo cells (wtHTLV-1) and 729pH6neo cells (wtHTLV-2) were cocultured with freshly isolated uninfected PBMCs for 9 weeks. The cultures were harvested, stained with anti-CD3, anti-CD4, and anti-CD8 antibodies, and analyzed by flow cytometry once every week. The percentages of $CD4^+$ and $CD8^+$ T cells within the $CD3^+$ T cell gate were determined and normalized to 100. The normalized $CD4^+$ T cells in the individual wells for both the viruses are plotted. Each well is represented by the corresponding symbol, for which the left *y* axis shows the percentage of $CD4^+$ T cells and the right *y* axis shows the percentage of $CD8^+$ T cells. (A) Longitudinal analysis of the T cell phenotype of wtHTLV-1- or wtHTLV-2-induced immortalization. Eight wells were analyzed at each time point for both viruses. The circles represent wtHTLV-1, and the triangles represent wtHTLV-2. The vertical bar represents the 95% confidence interval for each of the viruses at the given time points. The trend lines connect the estimated mean values in each of the two groups, which is an adjusted mean value from a generalized linear model. The differences in the mean values between wtHTLV-1 and wtHTLV-2 were statistically significant from week 4 onwards (week 4, $P = 0.04$; weeks 5 to 9, $P < 0.001$; generalized linear model with Tukey's method for multiplicity adjustment). (B) T cell phenotypic analysis of wtHTLV-1- or wtHTLV-2-induced immortalization after 9 weeks of coculture (remaining wells from data above). The bar represents the average percentage of T cells. The total number of wells analyzed and the average percentages (standard deviations [SD]) for both $CD4^+$ and $CD8^+$ T cells are indicated below. The percentage of wtHTLV-1-immortalized $CD4^+$ T cells was significantly higher than that of the wtHTLV-2-immortalized $CD4^+$ T cells ($P < 0.001$, *t* test).

8. However, *Hbz* mRNA expression (shown as open circles) peaked at week 8 along with the proviral loads. Therefore, *Hbz* mRNA expression was directly proportional to the proviral load ($r = 0.8$, $P = 0.002$). In the HTLV-2-infected rabbits, both *tax*/*rex* (shown as closed circles) and *Aph-2* (shown as open circles) transcripts followed the same pattern as the proviral load (shown as a gray area plot) and hence were directly proportional to the proviral load ($r = 0.9$, $P = 0.04$ for both transcripts).

Overall, the proviral loads were 4-fold (1 in 7 $CD4^+$ T cells and 1 in 1.7 $CD8^+$ T cells) and 9-fold (1 in 100 $CD4^+$ T cells and 1 in 11 $CD8^+$ T cells) higher in the $CD8^+$ T cells from HTLV-1- and HTLV-2-infected rabbits, respectively. Altogether, these data clearly show that, similar to the $CD4^+$ T cells, the $CD8^+$ T cells are also infected as early as week 1 postinoculation by both HTLV-1 and HTLV-2. Hence, there is no T cell preference by either HTLV-1 or HTLV-2 at this initial infection stage. Furthermore, in the $CD8^+$ T cells, HTLV-1-infected rabbits had a higher degree of infection than HTLV-2-infected rabbits. However, the patterns of the longitudinal proviral burden were similar in both HTLV-1- and HTLV-2-infected groups. In the HTLV-1-infected group, the early *tax*/*rex* mRNA expression positively regulates viral gene expression, resulting in a late proviral load peak. The late *Hbz* mRNA expression directly correlated with the proviral load, consistent with our previous report that HBZ helps in cell proliferation and viral persistence (2). In the HTLV-2-infected group, it is interesting to note that *Aph-2* mRNA expression was high, which was similar to *Hbz* mRNA expression in the HTLV-1-infected group. Although one study has shown APH-2 repression of Tax function (11), further *in vitro* and *in vivo* characterization of APH-2 in comparison to HBZ, its HTLV-1 counterpart could contribute to interesting pathogenic differences between HTLV-1 and HTLV-2.

HTLV-1 and HTLV-2 induced immortalization of $CD4^+$ and $CD8^+$ T cells. Our *in vivo* analysis in newly infected rabbits suggested that there was no distinct entry tropism displayed by HTLV-1 and HTLV-2, consistent with the conclusion that the envelope might dictate the distinct HTLV-1 and HTLV-2 tropism at a subsequent stage. To address this, we went back to our well-established *in vitro* immortalization assay to determine the CD4/CD8 phenotype of the HTLV-transformed T cells at weekly intervals, over a 9-week period. As expected, both wtHTLV-1 and wtHTLV-2 immortalized fresh PBMCs, and using p19 Gag production as a surrogate marker for virus infection and virion production, we showed that the immortalization was virus-mediated (data not shown). The PBMCs were stained and analyzed by flow cytometry at week 0 to determine the $CD4^+$ and $CD8^+$ T cell percentages in the starting target population. PBMCs were comprised of 56% $CD4^+$ T cells and 30% $CD8^+$ T cells (actual percentages). Subsequently, at each week, eight wells from cocultures with wtHTLV-1 or wtHTLV-2 were analyzed by flow cytometry. The raw numbers of positive $CD3^+$ $CD4^+$ T cells and $CD3^+$ $CD8^+$ T cells were normalized to 100. The normalized $CD4^+$ and $CD8^+$ T cell percentages at each time point for both the viruses were analyzed statistically in a generalized linear model (Fig. 4A). By week 2, the numbers of proliferating $CD4^+$ and $CD8^+$ T cells became proportional to each other. By week 4, there was a significant difference in the predominantly proliferating population of T cells (as shown by the error bars depicting the confidence intervals for each group) (Fig. 4A). This difference was statistically significant ($P = 0.04$). Over time, the separation between the predominant population and the other minor population increased steadily. This difference was statistically significant at all remaining time points—weeks 5 to 9 ($P < 0.001$). By week 9, wtHTLV-1

predominantly transformed $CD4^+$ T cells and wtHTLV-2 predominantly transformed $CD8^+$ T cells. This result at week 9 was confirmed by phenotyping the remaining proliferating wells immortalized/transformed by each of the viruses (Fig. 4B).

In summary, our data indicate that at the early time points postinoculation, both of the T cell populations were infected similarly *in vivo*. *In vitro*, both T cell populations proliferated proportionately at the initial time points, irrespective of the virus strain. However, over time, one type of T cell was selected for predominant clonal expansion: $CD4^+$ T cells for HTLV-1 and $CD8^+$ T cells for HTLV-2.

DISCUSSION

HTLV-1 and HTLV-2 proviruses have been detected in a number of hematopoietic cells in infected individuals (12, 19, 20, 22, 25, 29, 37). However, *in vitro* studies have shown the preferential transformation of $CD4^+$ T cells by HTLV-1 and $CD8^+$ T cells by HTLV-2 (30, 41, 42, 45). HTLV-1 recapitulates this preference *in vivo* in ATL patients, while there is no evidence for HTLV-2 being associated with leukemia *in vivo*. Since the initial establishment of infection in humans is generally asymptomatic and is followed by a clinical latency period of 2 to 4 decades, the ability of HTLV-1 to infect several hematopoietic cells and yet preferentially transform only $CD4^+$ T cells is poorly understood. An important question in this regard is whether preferential transformation of a select population occurs during the early infection stage or during the decades-long latency period. In humans, the time of infection with the virus is typically unknown. Therefore, in this study we used the rabbit model to determine the differential infection and replication abilities of HTLV-1 and HTLV-2 in $CD4^+$ and $CD8^+$ T cells during the first 12 weeks postinoculation. Our results provide the first evidence for the lack of $CD4^+$ or $CD8^+$ T cell preference exhibited by HTLV-1 or HTLV-2 during the early infection stage. This early longitudinal analysis provides novel information to our understanding of the early replication, mediated by Tax, and subsequent viral persistence, mediated by HBZ, in newly HTLV-1-infected hosts. We further determined the preferential tropism at the early transformation stage using the well-established *in vitro* immortalization assay system. Longitudinal analysis of the CD4/CD8 phenotype of the proliferating T cells in this assay indicated that the predominance of the preferred T cell type emerged after 4 to 5 weeks in culture, resulting in the selective clonal expansion of one T cell type over the other, depending on which virus strain was used to infect the cells. Since a previous study has indicated that the viral envelope encodes the genetic determinant of HTLV transformation tropism (42), these findings together suggest that the viral envelope mediates the clonal expansion of the selected T cell type during the decades-long clinical latency period.

Rabbits have been used extensively in the HTLV field to understand viral infection, persistence, and transmission and also the virus-triggered immune response (reviewed in reference 21). Although some studies have reported manifestation of disease in rabbits, the majority of the studies mimic the asymptomatic infection in humans. So far, we have utilized the rabbit model to understand the role of HTLV-1 and HTLV-2 accessory proteins (2, 5, 43, 44) and also to determine the replication kinetics of HTLV-1 in comparison with the *in vitro* immortalization assay (24). In the present study, we utilized the rabbit model to investigate the replication kinetics of HTLV-1 and HTLV-2 in the target T cell populations, highly purified $CD4^+$ and $CD8^+$ T cells, during the first 12 weeks of infection. Since our previous rabbit study showed that the proviral loads in the PBMCs declined or stabilized at a certain set point by the 8-week time point, we evaluated the infected rabbit T cells for 12 weeks in the present study. Rabbits, being outbred animals, showed similar trends rather than similar levels of infection and gene expression in our study, which is consistent with previous rabbit studies (4, 5, 16, 40, 43). Additionally, the proviral loads observed in this study were comparable to those in our previous HTLV-1 or HTLV-2 rabbit studies (2, 24, 43, 44). Therefore, the similar trends in the results support the conclusion that HTLV-1 and HTLV-2 infect both $CD4^+$ and $CD8^+$ T cells as early as week 1 postinoculation and establish a persistent infection in the next 2 to 4 weeks.

HTLV-2 is a less pathogenic virus than HTLV-1. Previous studies have shown that proviral loads in the PBMCs from HTLV-2-infected individuals were lower than in HTLV-1-infected individuals (18, 27, 28); however, these individuals were chronically infected for an unknown period of time. Additionally, HTLV-1 and HTLV-2 have been detected in both $CD4^+$ and $CD8^+$ T cells from individuals chronically infected with the corresponding viruses (12, 22, 37). It is not known whether this infection pattern is a result of long-term persistence in the host or whether these viruses can infect both T cell types upon early exposure to the virus. In this study, although HTLV-1 and HTLV-2 were capable of infecting both T cell types within 1 week postinoculation, the HTLV-1 burden was severalfold higher than the HTLV-2 burden over time. Thus, consistent with previous reports from chronically infected human PBMCs, we see a higher degree of infection with HTLV-1, even within the first 12 weeks postinoculation. The gene expression analysis also revealed more active replication with HTLV-1 than HTLV-2. In addition, HTLV-1 infected rabbit $CD4^+$ T cells more efficiently than HTLV-2. This difference is likely host cell receptor driven. Moreover, it was shown previously that the HTLV-2 envelope does not require HSPG for binding and entry into the cell. In contrast, the HTLV-2 envelope binds poorly to $CD4^+$ T cells, which is thought to be due to interference by the increased expression of HSPG on activated T cells (17). For the same reason, the $CD8^+$ T cells also carry a higher HTLV-1 burden than HTLV-2. There is an early enhancement of HSPG expression on $CD4^+$ T cells compared to a late increase on the $CD8^+$ T cells, upon activation (17); this time lag in receptor expression might contribute to the varied HTLV-1 proviral load pattern in the $CD4^+$ and $CD8^+$ T cells.

Based on our present findings and previously published reports by us and others (2, 9, 10, 12, 14, 17, 36, 39, 47), we have designed a schematic "working model" to interpret our data in the context of HTLV-1 (the more prevalent and pathogenic virus compared to HTLV-2) and the host (Fig. 5). Upon inoculation of an immunocompetent host with HTLV-1, the virus triggers an adaptive immune response over the first 4 weeks. The first adaptive immune response is the activation of $CD4^+$ T cells. This immune activation leads to the increased expression of HSPGs on the surface of the $CD4^+$ T cells, which subsequently facilitates HTLV-1 infection due to the requirement for HSPG by HTLV-1 to bind and enter cells (17). The increased availability of activated $CD4^+$ T cells results in an early peak in the proviral load (Fig. 2A), as the virus preferentially infects $CD4^+$ T cells (9). *tax*/*rex* mRNA, being completely spliced, is the first abundantly expressed transcript (36) in the infected cells, which feeds back into increasing

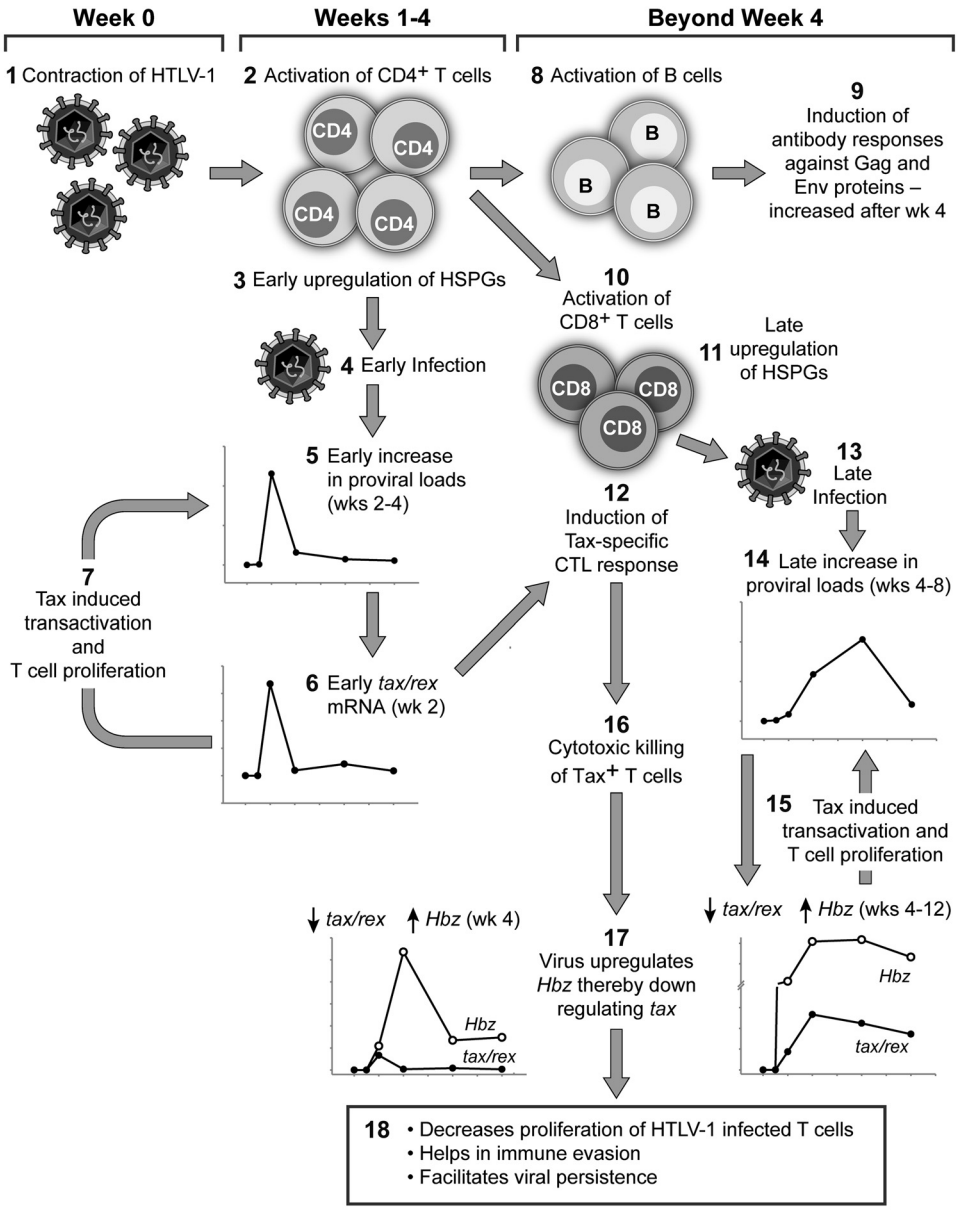

FIG 5 Sequential early events after HTLV-1 infection in an immunocompetent host. This model schematically depicts the early events in a HTLV-1-infected host. The Arabic numerals represent the sequential events in the model. (Event 1) Infection of the host with HTLV-1. (Event 2) Initial activation of helper $CD4^+$ T cells by HTLV-1. (Event 3) Activation increases HSPG expression on the surface of the $CD4^+$ T cells. (Event 4) The abundance of HSPGs on the surface increases HTLV-1 binding and entry into these activated HTLV-1-specific $CD4^+$ T cells. (Event 5) Infection results in an early increase in proviral load in these cells by weeks 2 to 4. (Event 6) Increased proviral load is reflected in early *tax*/*rex* mRNA expression, by week 2. (Event 7) Tax-induced viral transactivation and low-grade T cell proliferation also feed back into increasing the proviral loads. (Event 8) The activated HTLV-1-specific $CD4^+$ T cells activate B cells to induce antibody responses against Gag and Env proteins by week 4 (event 9) and activate $CD8^+$ T cells to induce cytotoxic killing of HTLV-1-infected cells (event 10). (Event 11) Activation of $CD8^+$ T cells leads to an increase of HSPG expression on their surface. (Event 12) Activation with simultaneously high levels of Tax induces Tax-specific CTL responses by week 4. (Event 13) HTLV-1 takes advantage of the late availability of HSPGs on the $CD8^+$ T cells. (Event 14) This results in a late proviral load peak by weeks 4 to 8. (Event 15) Fresh infection induces *tax*/*rex* mRNA expression, which in turn increases proviral loads by viral transactivation and low-grade T cell proliferation. (Event 16) Increased Tax expression induces cytotoxic killing of Tax^+ T cells. (Event 17) After week 4, the virus also alters its gene expression profile by reducing *tax*/*rex* mRNA and increasing *Hbz* mRNA expression. (Event 18) These sequential events result in decreased proliferation of HTLV-1-infected T cells, immune evasion, and long-term viral persistence.

the proviral loads by Tax-induced viral transactivation as well as low-grade T cell proliferation (10). Hence, the expression kinetics of *tax*/*rex* mRNA mirrors that of the proviral load at week 2 (as shown in Fig. 2C). In the meantime, the HTLV-1-specific helper $CD4^+$ T cells activate B cells and cytotoxic $CD8^+$ T cells (CTLs). The activated HTLV-1-specific B cells make neutralizing antibodies against HTLV-1 Gag and Env proteins, which were detected at high levels from week 4 onwards. Activated CTLs targeted against Tax-expressing cells are detectable by week 4 (14). These activated HTLV-1-specific CTLs also show increased HSPG expression on

their surface (17), which facilitates their preferential infection by HTLV-1 (12). The late activation of the $CD8^+$ T cells and the late expression of HSPGs on their surface result in the late proviral load peak (weeks 4 to 8) in these cells compared to $CD4^+$ T cells (Fig. 2A and 3A). Similar to the $CD4^+$ T cells, these infected $CD8^+$ T cells also express *tax*/*rex* mRNA initially (week 4), which in turn feeds back into virus production and increases the proviral loads (Fig. 3C). The early expression of Tax in the infected cells induces senescence soon after infection, resulting in the constant removal of infected cells with high levels of Tax expression (47). The abundance in Tax expression also induces cytotoxic killing of Tax-positive $CD4^+$ and $CD8^+$ T cells (12) by week 4. By week 4, the virus also shifts its gene expression profile by increasing *Hbz* and decreasing *tax*/*rex* transcripts (Fig. 2C and 3C). This simultaneous action of the host immune system as well as virus gene transcription results in the elimination of the Tax-positive cells, thereby decreasing new virion production for fresh infection and the proliferation of HTLV-1-infected T cells. This result is witnessed by the decline in the proviral loads and *tax*/*rex* mRNA expression in both the $CD4^+$ and $CD8^+$ T cells (Fig. 2A and C and 3A and C). The HTLV-1-specific CTLs carrying the virus have impaired lytic function (12), and hence the proviral loads persist longer in the $CD8^+$ T cells (weeks 4 to 8). HBZ plays an important role in viral persistence (2) by competitively decreasing Tax expression; this rescues cells from Tax-induced senescence (47) as well as from the Tax-specific CTL lysis. Additionally, HBZ-specific CTLs do not efficiently lyse their target cells (39). The initial burst of $CD4^+$ helper T cell response to activate prolonged B cell and $CD8^+$ cytotoxic T cell responses in any given viral infection probably influences the proviral load kinetics inadvertently due to the circumstantial availability of activated target cells. These sequentially concerted events over time lead to long-term low-grade viral persistence in a newly infected immunocompetent host.

Preferential *in vitro* transformation of $CD4^+$ and $CD8^+$ T cells by HTLV-1 and HTLV-2, respectively, has been well documented (41, 42, 45). This differential tropism and distinct pathobiology between HTLV-1 and HTLV-2 warrants comparative studies between these two viruses in order to understand HTLV-1-mediated leukemogenesis. The 2- to 4-decade clinical latency period between initial infection and ATL manifestation is the main drawback that hinders experimental evaluation of the underlying oncogenic mechanism. Since our rabbit study revealed the lack of preferential entry of HTLV-1 or HTLV-2 into $CD4^+$ or $CD8^+$ T cells, we next tested the possibility of this preferential tropism being conferred at the initial infection and subsequent transformation stage using the *in vitro* immortalization assay, which is a well-accepted method to evaluate this pathogenic characteristic of HTLV in an experimental time frame. In this study, both $CD4^+$ and $CD8^+$ T cells proliferated in equal proportions by week 2, indicating that both HTLV-1 and HTLV-2 have immortalized both T cell types. However, it is not possible to suggest equal transformation at this time point because the observed percentages of the proliferating T cells are a balance between uninfected dying cells and HTLV-infected immortalized cells. Beyond week 3, the constant p19 Gag production is indicative of HTLV-induced proliferation. The predominance of HTLV-1-immortalized $CD4^+$ T cells and HTLV-2-immortalized $CD8^+$ T cells emerged at weeks 4 to 5, which continued to increase for the remaining period of the experiment. This result confirms our hypothesis that the predominance of one particular type of T cell in HTLV-1- or HTLV-2-immortalized cultures results from selective clonal expansion. Since there are no animal models for studying HTLV-1 disease outcomes so far, the *in vitro* immortalization assay is the best available assay to study the transformation stage in HTLV-1 pathogenesis. The added advantage is the ability to directly compare HTLV-2, which is aleukemic *in vivo*. Although the *in vitro* immortalization of T cells likely is correlated to T cells in infected asymptomatic carriers, the results need to be interpreted cautiously due to the lack of immune surveillance *in vitro* and the unaccounted for environmental factors in the milieu of the complex human system.

In summary, HTLV-1 and HTLV-2 established a persistent infection in the $CD4^+$ and $CD8^+$ T cells of rabbits, at levels comparable to the PBMC loads from previous studies. By week 1 postinoculation, both viruses were detectable in both $CD4^+$ and $CD8^+$ T cell populations. Consistent with reports in humans, HTLV-1 established a more robust infection in both $CD4^+$ and $CD8^+$ T cells, compared to HTLV-2. In the $CD4^+$ T cells from HTLV-1-infected rabbits, the early proviral load mirrored the abundant early *tax*/*rex* mRNA expression. This pattern was observed in neither the $CD8^+$ T cells from HTLV-1-infected rabbits nor in the HTLV-2-infected rabbit $CD4^+$ and $CD8^+$ T cells. Whether the early high-level Tax expression contributes to the distinct $CD4^+$ T cell malignancy resulting from HTLV-1 infection requires further exploration. *Hbz* mRNA expression, being abundant in the latter part of the experimental time course in both the T cell types, reiterates the role of HBZ in viral persistence. The HTLV-2 counterpart, *Aph-2* mRNA, in the $CD8^+$ T cells followed the same replication kinetics as *Hbz* mRNA in HTLV-1-infected rabbits, but not in their $CD4^+$ T cells. Future comparative studies are warranted to dissect the role of APH-2 in viral persistence that may lead to distinct viral pathogenesis. The crux of our *in vivo* findings is that HTLV-1 and HTLV-2 do not exhibit any preference to infect the target populations, $CD4^+$ and $CD8^+$ T cells, at the initial infection stage. Furthermore, the *in vitro* immortalization assay revealed that HTLV-1 and HTLV-2 induce proliferation of both $CD4^+$ and $CD8^+$ T cells by week 2. The preferential predominance of the $CD4^+$ T cells in HTLV-1-immortalized cultures and the $CD8^+$ T cell predominance in HTLV-2-immortalized cultures resulted from selective outgrowth of the preferred clonal population beyond week 4. Thus, the viral envelope, which has been shown to dictate transformation tropism in culture, probably plays an important role along with other players, like Tax, to mediate the preferential T cell transformation tropism. Our findings in this study provide important insight into the HTLV-mediated transformation process and open new venues to explore the underlying mechanisms in HTLV-1-mediated leukemogenesis using this *in vitro* immortalization assay as a valuable research tool.

ACKNOWLEDGMENTS

We thank Snehalata Gupta and Robyn Haines for help with rabbit handling, Kate Hayes-Ozello for editing, and Tim Vojt for figure preparation.

This work was supported by grants from the National Institutes of Health (CA100730 and CA077556) to P.L.G.

REFERENCES

1. **Araujo A, Hall WW.** 2004. Human T-lymphotropic virus type II and neurological disease. Ann. Neurol. **56**:10–19.

2. **Arnold J, et al.** 2006. Enhancement of infectivity and persistence in vivo by HBZ, a natural antisense coded protein of HTLV-1. Blood **107**:3976–3982.
3. **Bartman MT, et al.** 2008. Long-term increases in lymphocytes and platelets in human T-lymphotropic virus type II infection. Blood **112**:3995–4002.
4. **Bartoe JT, et al.** 2000. Functional role of pX open reading frame II of human T-lymphotropic virus type 1 in maintenance of viral loads in vivo. J. Virol. **74**:1094–1100.
5. **Cockerell GL, Rovank J, Green PL, Chen ISY.** 1996. A deletion in the proximal untranslated pX region of human T-cell leukemia virus type II decreases viral replication but not infectivity in vivo. Blood **87**:1030–1035.
6. **Gessain A, et al.** 1985. Antibodies to human T-lymphotropic virus type-I in patients with tropical spastic paraparesis. Lancet **ii**:407–410.
7. **Ghez D, Lepelletier Y, Jones KS, Pique C, Hermine O.** 2010. Current concepts regarding the HTLV-1 receptor complex. Retrovirology **7**:99.
8. **Ghez D, et al.** 2006. Neuropilin-1 is involved in human T-cell lymphotropic virus type 1 entry. J. Virol. **80**:6844–6854.
9. **Goon PK, et al.** 2004. Human T cell lymphotropic virus type I (HTLV-I)-specific CD4+ T cells: immunodominance hierarchy and preferential infection with HTLV-I. J. Immunol. **172**:1735–1743.
10. **Grassmann R, Aboud M, Jeang KT.** 2005. Molecular mechanisms of cellular transformation by HTLV-1 Tax. Oncogene **24**:5976–5985.
11. **Halin M, et al.** 2009. Human T-cell leukemia virus type 2 produces a spliced antisense transcript encoding a protein that lacks a classic bZIP domain but still inhibits Tax2-mediated transcription. Blood **114**:2427–2438.
12. **Hanon E, et al.** 2000. Fratricide among CD8(+) T lymphocytes naturally infected with human T cell lymphotropic virus type I. Immunity **13**:657–664.
13. **Hattori T, Uchiyama T, Toibana T, Takatsuki K, Uchino H.** 1981. Surface phenotype of Japanese adult T-cell leukemia cells characterized by monoclonal antibodies. Blood **58**:645–647.
14. **Haynes RA, II, Phipps AJ, Yamamoto B, Green P, Lairmore MD.** 2009. Development of a cytotoxic T-cell assay in rabbits to evaluate early immune response to human T-lymphotropic virus type 1 infection. Viral Immunol. **22**:397–405.
15. **Hinuma Y, et al.** 1981. Adult T-cell leukemia: antigen in an ATL cell line and detection of antibodies to the antigen in human sera. Proc. Natl. Acad. Sci. U. S. A. **78**:6476–6480.
16. **Hiraragi H, et al.** 2006. Human T-lymphotropic virus type 1 mitochondrion-localizing protein p13(II) is required for viral infectivity in vivo. J. Virol. **80**:3469–3476.
17. **Jones KS, et al.** 2006. Human T-cell leukemia virus type 1 (HTLV-1) and HTLV-2 use different receptor complexes to enter T cells. J. Virol. **80**:8291–8302.
18. **Kira J, et al.** 1991. Increased HTLV-I proviral DNA in HTLV-I-associated myelopathy; a quantitative polymerase reaction study. Ann. Neurol. **29**:194–201.
19. **Knight SC, Macatonia SE, Cruickshank K, Rudge P, Patterson S.** 1993. Dendritic cells in HIV-1 and HTLV-1 infection. Adv. Exp. Med. Biol. **329**:545–549.
20. **Koyanagi Y, et al.** 1993. In vivo infection of human T-cell leukemia virus type I in non-T cells. Virology **196**:25–33.
21. **Lairmore MD, Silverman L, Ratner L.** 2005. Animal models for human T-lymphotropic virus type 1 (HTLV-1) infection and transformation. Oncogene **24**:6005–6015.
22. **Lal RB, Owen SM, Rudolph DL, Dawaon C, Prince H.** 1995. In vivo cellular tropism of human T-cell lymphotrophic virus type-II is not restricted to CD8+ cells. Virology **210**:441–447.
23. **Li M, Green PL.** 2007. Detection and quantitation of HTLV-1 and HTLV-2 mRNA species by real-time RT-PCR. J. Virol. Methods **142**:159–168.
24. **Li M, Kesic M, Yin H, Lianbo Y, Green P.** 2009. Kinetic analysis of human T-cell leukemia virus type 1 gene expression in cell culture and infected animals. J. Virol. **83**:3788–3797.
25. **Macatonia SE, Cruickshank JK, Rudge P, Knight SC.** 1992. Dendritic cells from patients with tropical spastic paraparesis are infected with HTLV-1 and stimulate autologous lymphocyte proliferation. AIDS Res. Hum. Retroviruses **8**:1699–1706.
26. **Manel N, et al.** 2003. The ubiquitous glucose transporter GLUT-1 is a receptor for HTLV. Cell **115**:449–459.
27. **Manns A, et al.** 1999. Quantitative proviral DNA and antibody levels in the natural history of HTLV-I infection. J. Infect. Dis. **180**:1487–1493.
28. **Murphy EL, et al.** 2004. Higher human T lymphotropic virus (HTLV) provirus load is associated with HTLV-I versus HTLV-II, with HTLV-II subtype A versus B, and with male sex and a history of blood transfusion. J. Infect. Dis. **190**:504–510.
29. **Nath MD, Ruscetti FW, Petrow-Sadowski C, Jones KS.** 2003. Regulation of the cell-surface expression of an HTLV-I binding protein in human T cells during immune activation. Blood **101**:3085–3092.
30. **Newbound GC, Andrews JM, O'Rourke JP, Brady JN, Lairmore MD.** 1996. Human T-cell lymphotropic virus type 1 Tax mediates enhanced transcription in CD4+ T-lymphocytes. J. Virol. **70**:2101–2106.
31. **Orland JR, et al.** 2003. Prevalence and clinical features of HTLV neurologic disease in the HTLV Outcomes Study. Neurology **61**:1588–1594.
32. **Osame M, et al.** 1986. HTLV-I associated myelopathy, a new clinical entity. Lancet **i**:1031–1032.
33. **Pinon JD, et al.** 2003. Human T-cell leukemia virus type 1 envelope glycoprotein gp46 interacts with cell surface heparan sulfate proteoglycans. J. Virol. **77**:9922–9930.
34. **Poiesz BJ, et al.** 1980. Detection and isolation of type C retrovirus particles from fresh and cultured lymphocytes of a patient with cutaneous T-cell lymphoma. Proc. Natl. Acad. Sci. U. S. A. **77**:7415–7419.
35. **Proietti FA, Carneiro-Proietti AB, Catalan-Soares BC, Murphy EL.** 2005. Global epidemiology of HTLV-I infection and associated diseases. Oncogene **24**:6058–6068.
36. **Rende F, et al.** 2011. Kinetics and intracellular compartmentalization of HTLV-1 gene expression: nuclear retention of HBZ mRNA. Blood **117**:4855–4859.
37. **Richardson JH, Edwards AJ, Cruickshank JK, Rudge P, Dalgleish AG.** 1990. In vivo cellular tropism of human T-cell leukemia virus type 1. J. Virol. **64**:5682–5687.
38. **Roucoux DF, Murphy EL.** 2004. The epidemiology and disease outcomes of human T-lymphotropic virus type II. AIDS Rev. **6**:144–154.
39. **Suemori K, et al.** 2009. HBZ is an immunogenic protein, but not a target antigen for human T-cell leukemia virus type 1-specific cytotoxic T lymphocytes. J. Gen. Virol. **90**:1806–1811.
40. **Valeri VW, et al.** 2010. Requirement of the human T-cell leukemia virus p12 and p30 genes for infectivity of human dendritic cells and macaques but not rabbits. Blood **116**:3809–3817.
41. **Wang T-G, Ye J, Lairmore M, Green PL.** 2000. In vitro cellular tropism of human T-cell leukemia virus type 2. AIDS Res. Hum. Retroviruses **16**:1661–1668.
42. **Xie L, Green PL.** 2005. Envelope is a major viral determinant of the distinct in vitro cellular transformation tropism of human T-cell leukemia virus type 1 (HTLV-1) and HTLV-2. J. Virol. **79**:14536–14545.
43. **Yamamoto B, et al.** 2008. Human T-cell leukemia virus type 2 post-transcriptional control protein p28 is required for viral infectivity and persistence in vivo. Retrovirology **5**:38.
44. **Ye J, Silverman L, Lairmore MD, Green PL.** 2003. HTLV-1 Rex is required for viral spread and persistence in vivo but is dispensable for cellular immortalization in vitro. Blood **102**:3963–3969.
45. **Ye J, Xie L, Green PL.** 2003. Tax and overlapping Rex sequences do not confer the distinct transformation tropisms of HTLV-1 and HTLV-2. J. Virol. **77**:7728–7735.
46. **Yoshida M, Miyoshi I, Hinuma Y.** 1982. Isolation and characterization of retrovirus from cell lines of human adult T-cell leukemia and its implication in the disease. Proc. Natl. Acad. Sci. U. S. A. **79**:2031–2035.
47. **Zhi H, et al.** 2011. NF-kappaB hyper-activation by HTLV-1 tax induces cellular senescence, but can be alleviated by the viral anti-sense protein HBZ. PLoS Pathog. **7**:e1002025.